PCCP

How to Add a Five-Membered Ring to Polycyclic Aromatic Hydrocarbons (PAHs) – Molecular Mass Growth of the 2-Naphthyl Radical ($C_{10}H_7$) to Benzindenes ($C_{13}H_{10}$) as a Case Study

Journal:	*Physical Chemistry Chemical Physics*
Manuscript ID	CP-ART-05-2019-002930.R1
Article Type:	Paper
Date Submitted by the Author:	10-Jul-2019
Complete List of Authors:	Zhao, Long; University of Hawaii at Manoa, Department of Chemistry Prendergast, Matthew; University of Hawai'i at Manoa Kaiser, Ralf I; University of Hawaii, Xu, Bo; Lawrence Berkeley National Laboratory, Chemical Sciences Division Ablikim, Utuq; E O Lawrence Berkeley National Laboratory, Chemical Dynamics; Kansas State University, Physics Lu, Wenchao; b. Chemical Sciences Division, Lawrence Berkeley National Laboratory Ahmed, Musahid; Lawrence Berkeley National Laboratory, Chemical Sciences Division Oleinikov, Artem; Samara National Research University Azyazov, Valeriy; Samara National Research University; Lebedev Physical Institute of RAS, Department of Chemical & Electric Discharge Lasers Howlader, A.; Florida International University, Department of Chemistry and Biochemistry Wnuk, Stanislaw; Florida International University, Chemistry and Biochemistry Mebel, Alexander; Florida International University, Chemistry and Biochemistry

How to Add a Five-Membered Ring to Polycyclic Aromatic Hydrocarbons (PAHs) – Molecular Mass Growth of the 2-Naphthyl Radical ($C_{10}H_7$) to Benzindenes ($C_{13}H_{10}$) as a Case Study

Long Zhao, Matthew Prendergast, Ralf. I. Kaiser*
Department of Chemistry, University of Hawaii at Manoa, Honolulu, HI 96822, USA

Bo Xu, Utuq Ablikim, Wenchao Lu, Musahid Ahmed*
Chemical Sciences Division, Lawrence Berkeley National Laboratory, Berkeley, CA 94720, USA

Artem D. Oleinikov, Valeriy N. Azyazov
Samara National Research University, Samara 443086, Russia

A. Hasan Howlader, Stanislaw F. Wnuk
Department of Chemistry and Biochemistry, Florida International University, Miami, FL 33199, USA

Alexander M. Mebel*
Department of Chemistry and Biochemistry, Florida International University, Miami, FL 33199, USA
and Samara National Research University, Samara 443086, Russia

Phys. Chem. Chem. Phys. (submitted 2019)

ABSTRACT

The three-ring polycyclic aromatic hydrocarbons (PAHs) 3*H*-benz[*e*]indene ($C_{13}H_{10}$) and 1*H*-benz[*f*]indene ($C_{13}H_{10}$) along with their naphthalene-based isomers 2-(prop-2-yn-1-yl)naphthalene ($C_{13}H_{10}$), 2-(prop-1-yn-1-yl)naphthalene ($C_{13}H_{10}$), and 2-(propa-1,2-dien-1-yl)naphthalene ($C_{13}H_{10}$) were formed through a "directed synthesis" via a high temperature chemical micro reactor under combustion-like conditions (1300 ± 35 K) through the reactions of the 2-naphthyl isomer ($C_{10}H_7^{\bullet}$) with allene (C_3H_4) and methylacetylene (C_3H_4). The isomer distributions were probed utilizing tunable vacuum ultraviolet radiation from the Advanced Light Source (ALS) by recording the photoionization efficiency curves at mass-to-charge of m/z = 166 ($C_{13}H_{10}$) and 167 ($^{13}CC_{12}H_{10}$) of the products in a supersonic molecular beam. Complemented by electronic structure calculations, our study reveals critical mass growth processes via annulation of a five-membered ring from the reaction between aryl radicals and distinct C_3H_4 isomers at elevated temperatures as present in combustion processes and in circumstellar envelopes of carbon stars. The underlying reaction mechanisms proceed through the initial addition of the 2-naphthyl radical with its radical center to the π-electron density of the allene and methylacetylene reactants via entrance barriers between 8 and 14 kJ mol^{-1}, followed by isomerization (hydrogen shifts, ring closure), and termination via atomic hydrogen losses accompanied by aromatization. The reaction mechanisms reflect the formation of indene – the prototype PAH carrying a single five- and a single six-membered ring – synthesized through the reaction of the phenyl radical ($C_6H_5^{\bullet}$) with allene and methylacetylene. This leads us to predict that aryl radicals – upon reaction with allene/methylacetylene – may undergo molecular mass growth processes via ring annulation and de-facto addition of a five-membered ring to form molecular building blocks essential to transit planar PAHs out of the plane.

1. Introduction

Molecular beam experiments with crossed beams[1-5] and pyrolytic micro reactors[6-9] critically aid in fundamental understanding of the formation mechanisms of polycyclic aromatic hydrocarbons (PAHs)[10-24] along with their methylated counterparts carrying up to four six-membered rings. They have provided profound insight of complementary hydrogen abstraction – acetylene addition (HACA)[25, 26] and hydrogen abstraction – vinylacetylene addition (HAVA) pathways in combustion[27-29] and extraterrestrial environments[30] (Schemes 1 and 2). These PAHs are synthesized through systematic ring annulation reactions starting with aromatic radicals like benzyl ($C_7H_7^{\bullet}$), phenyl ($C_6H_5^{\bullet}$), and naphthyl ($C_{10}H_7^{\bullet}$) reacting with acetylene (C_2H_2, HACA) and vinylacetylene (C_4H_4, HAVA) with the potential of yielding ultimately *two-dimensional graphene-type nanostructures*.[31] The elementary reactions involving acetylene (HACA) involve significant entrance barriers ranging from 10 to 30 kJ mol^{-1} and hence may only operate at elevated temperatures of up to a few 1,000 K such as in combustion flames[25, 26, 32] and in circumstellar envelopes of carbon rich Asymptotic Giant Branch (AGB) stars like IRC+10216. However, most of the studied reactions of aromatic radicals with vinylacetylene (HAVA) have been found to be essentially barrierless. Overall these bimolecular reactions are characterized by the initial formation of a van-der-Waals complex, addition of the radical center to the terminal carbon atom of the vinyl (H_2C=CH-) moiety of vinylacetylene leading to resonantly stabilized free radical intermediates (RSFRs) on the doublet surface, and eventually form PAHs after isomerization via ring closure and hydrogen shift(s) terminated by atomic hydrogen loss and aromatization.[27-29, 33] Therefore, in strong contrast to HACA, PAH growth via HAVA is rapid even at ultralow temperatures such as in cold molecular clouds like the Taurus Molecular Cloud-1 (TMC-1)[33] and also in hydrocarbon rich atmospheres of planets and their moons such as Saturn's satellite Titan[27] thus contradicting prior knowledge that high temperature environments are essential in the formation and growth of aromatic structures.[34]

However, whereas a systematic understanding of the formation of two-dimensional PAHs carrying solely six-membered rings up to pyrene ($C_{16}H_{10}$) is beginning to emerge,[27] the most fundamental reaction mechanisms leading eventually to *three-dimensional nanostructures* and soot in combustion systems are still unknown.[34] This requires an intimate understanding of how the simplest building blocks – precursors to non-planar aromatic molecules - are generated in the gas phase. It is critical to point out that non-planar PAHs such as corannulene along with fullerenes

(Scheme 3) require five-membered rings as found in, for example, indene (C_9H_8) to transit planar PAHs out of the plane. The intimate knowledge of the elementary mechanisms to synthesize PAHs carrying five-membered ring(s) is therefore critical to our understanding of the early stage chemistry of how three-dimensional (bowl-shaped) nanostructures and ultimately soot particles are formed in high temperature extreme environments such as in combustion systems and also in the interstellar medium (ISM). Once again, molecular beam experiments along with electronic structure calculations have been instrumental in untangling the formation of the simplest prototype of a PAH carrying a single six- and five-membered ring: indene (C_9H_8) (Scheme 2). Here, the benzyl radical ($C_7H_7^{\bullet}$) was found to react with acetylene (C_2H_2) yielding solely indene;[35] likewise, crossed molecular beams and high temperature chemical reactor studies provided evidence that the phenyl radical reacts with allene (C_3H_4) and methylacetylene (C_3H_4) forming indene (C_9H_8)[9, 36-39] along with non-PAH isomers phenylallene (C_9H_8), 1-phenyl-1-propyne (C_9H_8), and 3-phenyl-1-propyne (C_9H_8). Supported by electronic structure calculations, the successful study of the elementary reaction of 1-naphthyl ($C_{10}H_7^{\bullet}$) with acetylene (C_2H_2) provided the very first experimental evidence of a PAH carrying two six-membered and one five-membered rings: acenaphthylene ($C_{12}H_8$).[40] Overall, these studies revealed that elementary reactions of acetylene and allene/methylacetylene with aromatic radicals can 'add' a five-membered ring to an existing six-membered ring. However, the inherent elementary steps, energy flow processes, and reaction mechanisms to form more complex PAHs carrying five-membered rings via ring annulation of existing aromatic radicals leading to benzindene isomers (Scheme 4) at the molecular level are still elusive as detailed synthetic routes have not been investigated experimentally to date. A critical PAH carrying a five-membered ring – benzindene ($C_{13}H_{10}$) - has been detected in combustion flames of toluene[41-43] and benzene[44].

Although these isomers were probed in low pressure premixed toluene/oxygen/argon,[41, 42] in atmospheric pressure ethylene,[45, 46] and in benzene flames,[44] there is a paucity in the proposed reaction mechanisms. Those considered are suggested to involve unstudied multi step reactions of benzene (C_6H_6) or phenyl ($C_6H_5^{\bullet}$) with the benzyl radical ($C_7H_7^{\bullet}$) – after hydrogen abstractions - by closure of a new five-membered ring.[42, 44] 3*H*-benz[*e*]indene is proposed to be synthesized from 1-methylnaphthalene involving hydrogen abstraction from the methyl group followed by acetylene reaction, isomerization, and hydrogen loss.[44, 47-57] Here, we elucidate both experimentally and computationally the hitherto elusive pathways to three distinct isomers of benzindene ($C_{13}H_{10}$)

(Scheme 4). This is accomplished by exploring the chemistry of the elementary reactions of the 2-naphthyl radical ($C_{10}H_7^{\bullet}$), generated via pyrolysis of its 2-iodonaphthalene precursor, with two distinct C_3H_4 isomers - allene and methylacetylene – and probing the molecular mass growth processes via ring annulation to benzindenes along with its non-indene isomers 2-(prop-2-yn-1-yl)naphthalene, 2-(prop-1-yn-1-yl)naphthalene, and 2-(propa-1,2-dien-1-yl)naphthalene. The products were detected isomer-specifically through fragment-free photoionization in a molecular beam via tunable vacuum ultraviolet (VUV) light in tandem with the detection of the ionized molecules in a reflectron time-of-flight mass spectrometer thus shedding light on the synthesis of distinct benzindene isomers under high temperature conditions relevant to combustion settings and circumstellar envelopes of carbon-rich stars. Note that naphthalene ($C_{10}H_8$) has been identified in sooting flames of non-aromatic hydrocarbon-based fuels methane (CH_4),[58] ethane (C_2H_6),[59] acetylene (C_2H_2),[60] propene (C_3H_6),[61] *n*-butane (C_4H_{10}),[62] 1,3-butadiene (C_4H_6),[63] as well as in aromatic fuels such as benzene (C_6H_6),[41, 64] toluene (C_7H_8),[41, 42, 65] styrene (C_8H_8),[41] ethylbenzene (C_8H_{10}),[41, 66] and in xylenes (C_8H_{10}).[41, 67, 68] Unimolecular decomposition of naphthalene ($C_{10}H_8$) via hydrogen loss reaction or hydrogen atom abstraction from naphthalene by another radical can lead to the 2-naphthyl radical reactant ($C_{10}H_7^{\bullet}$) in these high temperature environments.

2. Experimental

By studying the reactions of the 2-naphthyl radical ($C_{10}H_7^{\bullet}$) with methylacetylene (CH_3CCH; Organic Technologies; 99%) and allene (H_2CCCH_2; Organic Technologies; 98%) under simulated combustion conditions, we deliver experimental and computational evidence of the growth of a five-membered ring connected to a naphthalene moiety. Here, a continuous beam of 2-naphthyl radicals ($C_{10}H_7^{\bullet}$) was prepared in situ through pyrolysis of the 2-iodonaphthalene ($C_{10}H_7I$) precursor (Sigma Aldrich, 99%). In separate experiments, the precursor was seeded in pure helium (blank experiment) and in the methylacetylene as well as allene reactants at pressures of 300 Torr. Each gas mixture was then expanded into a resistively heated silicon carbide (SiC) tube (“pyrolytic reactor”) held at 1275 ± 10 K (methylacetylene) and 1325 ± 10 K (allene). The hydrocarbon molecules introduced at typical pressures of 300 Torr do not only serve as a seeding gas, but also as reactants with the pyrolytically generated 2-naphthyl radicals. The products formed in the reactor were expanded supersonically, passed through a 2 mm diameter skimmer located 10 mm downstream of the pyrolytic reactor, and entered into the main chamber, which houses the Wiley–

McLaren reflectron time-of-flight mass spectrometer (ReTOF-MS). The quasi-continuous tunable vacuum ultraviolet (VUV) light from the Advanced Light Source intercepted the neutral molecular beam perpendicularly in the extraction region of the Re-TOF-MS. VUV single photon ionization is essentially a fragment-free ionization technique and is compared soft to electron impact ionization.[69] The ions formed via photoionization are extracted and detected by a multichannel plate detector. Photoionization efficiency (PIE) curves, which report ion counts as a function of photon energy with a step interval of 0.05 eV at a well-defined mass-to-charge ratio (*m/z*), were produced by integrating the signal recorded at the specific *m/z* for the species of interest from 8.00 eV to 10.00 eV. PIE calibration curves for six helium-seeded $C_{13}H_{10}$ isomers were also collected (Figure 1), to identify the products of interest observed in this work. Synthesis and characterization of 3*H*-benz[*e*]indene **p2,** 2-(prop-1-yn-1-yl)naphthalene **p4**, 2-(propa-1,2-dien-1-yl)naphthalene **p5**, and 2-(prop-2-yn-1-yl)naphthalene **p6** are described in the Electronic Supplementary Information (ESI).

3. Computational

The calculation of the energies and molecular parameters of various intermediates and transition states for the reactions of 2-naphthyl with allene and methylacetylene occurring on the $C_{13}H_{11}$ potential energy surface (PES), as well as of the reactants and possible products were carried out at the G3(MP2,CC)//B3LYP/6-311G(d,p) level of theory. Within this theoretical scheme, geometries were optimized and vibrational frequencies were calculated using the density functional B3LYP method with the 6-311G(d,p) method. Then, single-point total energies were improved using a series of coupled clusters CCSD(T) and second-order Møller-Plesset perturbation theory MP2 calculations, and the final energy was computed as

E[G3(MP2,CC)] = E[CCSD(T)/6-311G(d,p)] + E[MP2/G3Large)] – E[MP2/6-311G(d,p)] + ZPE[B3LYP/6-311G(d,p)][70-72]

The G3(MP2,CC) model chemistry approach normally provides chemical accuracy of 0.01–0.02 Å for bond lengths, 1–2º for bond angles, and 3–6 kJ mol^{-1} for relative energies of hydrocarbons, their radicals, reaction energies, and barrier heights in terms of average absolute deviations.[71] The GAUSSIAN 09[73] and MOLPRO 2010[74] program packages were employed for the ab initio calculations. Phenomenological rate constants for the 2-naphthyl + C_3H_4 reactions at different temperatures and pressures were evaluated using the Rice-Ramsperger-Kassel-Marcus Master

Equation (RRKM-ME) theoretical approach as implemented in the MESS software package.[75, 76] The Rigid-Rotor, Harmonic-Oscillator (RRHO) model was generally adopted for the calculations of densities of states and partition functions for local minima and numbers of states for transition states. For critical entrance transition states of the $C_{10}H_7$ plus C_3H_4 reactions, low-frequency normal modes corresponding to internal rotations were treated as one-dimensional hindered rotors in partition function calculations, where the corresponding vibrational frequencies were removed. Respective one-dimensional torsional potentials were calculated by scanning PESs at the B3LYP/6-311G(d,p) level of theory. Tunneling corrections using asymmetric Eckart potentials were included in rate constant calculations. We adopted collision parameters used by us earlier for RRKM-ME calculations of the prototype C_6H_5 plus C_3H_4 reactions.[77] In particular, the Lennard-Jones parameters were taken as (ε/cm^{-1}, σ/Å) = (390, 4.46) and the temperature dependence of the range parameter α for the deactivating wing of the energy transfer function was expressed as $\alpha(T) = \alpha_{300}(T/300\ \mathrm{K})^n$, with n = 0.62 and α_{300} = 424 cm^{-1}. Calculations at very low pressures emulating the zero-pressure limit took into account radiational stabilization of $C_{13}H_{11}$ intermediates. Additional details of RRKM-ME calculations can be found in our previous publications[77] and in the input file for the MESS package given in the ESI.

4. Results & Discussion

4.1. Experiments

Figure 2 displays representative mass spectra recorded at a photoionization energy of 9.50 eV for the 2-naphthyl-helium, 2-naphthyl-allene, and 2-naphthyl-methylacetylene systems. In the reference system (Fig. 2a), ion counts can be seen at mass-to-charge (*m/z*) of 128, 129, 254, and 255. Signal at *m/z* = 254 and 255 can be linked to the molecular parent and the ^{13}C counterpart of the 2-iodonaphthalene precursor ($C_{10}H_7I$, $^{13}CC_9H_7I$). The ion counts at *m/z* = 128 and 129 could be associated with molecules holding the molecular formulae $C_{10}H_8$ and $^{13}CC_9H_8$. Upon introducing allene and methylacetylene into the reactor, additional ion counts emerge in both systems at *m/z* = 142, 143, 152, 153, 166, and 167 (Figs 2b and c). Accounting for the molecular weight of the methylacetylene/allene reactants and the products, the $C_{13}H_{10}$ isomer(s) (166 amu) plus atomic hydrogen along with their ^{13}C counterpart(s) are formed via the reaction of the 2-naphthyl radical (127 amu) plus allene/methylacetylene (40 amu). Signal at *m/z* = 142, 143, 152, and 153 likely originates from C_9H_{10}, $^{13}CC_8H_{10,}$ $C_{11}H_{10}$, and $^{13}CC_{10}H_{10}$, respectively.

Using PIE curves for *m/z* = 166, which is connected to the formation of $C_{13}H_{10}$ species, we now identify the structural isomer(s) synthesized in our reactor (Figure 3). These functions can be fit with a linear combination of established reference PIE curves for distinct $C_{13}H_{10}$ isomers (Figure 1). For the 2-naphthyl-allene (Fig. 3a) and 2-naphthyl-methylacetylene systems (Fig. 3c), the PIE curves at *m/z* = 166 can be both replicated with a linear combination of four reference curves of distinct $C_{13}H_{10}$ isomers. In case of the allene reactant, 3*H*-benz[*e*]indene (22 ± 5%), 1*H*-benz[*f*]indene (22 ± 5%), 2-(prop-2-yn-1-yl)naphthalene (11 ± 3%) and 2-(prop-1,2-dien-1-yl)naphthalene (45 ± 9%) are necessary to fit the experimental PIE curve with the contributions of the ion counts given in parentheses. The onset of 3*H*-benz[*e*]indene parent ion is experimentally calibrated to be 7.55 ± 0.05 eV; this corresponds well with the experimentally derived PIE curve at *m/z* = 166 with an onset of 7.60 ± 0.05 eV. On the other hand, for the methylacetylene reactant, contributions of 3*H*-benz[*e*]indene (5 ± 1%), 1*H*-benz[*f*]indene (11 ± 2%), 2-(pro-1-yn-1-yl)naphthalene (32 ± 6%) and 2-(prop-1,2-dien-1-yl)naphthalene (52 ± 10%) are necessary. For both systems, ion counts at *m/z* = 167 ($^{13}CC_{12}H_{10}$) represent the ^{13}C isotopologues of $C_{13}H_{10}$ since after scaling, the PIE graphs for *m/z* = 166 and 167 essentially overlap. It is important to highlight that in neither system, the 1*H*-benz[*e*]indene isomer was detected.

For completeness – and to provide additional information of the underlying reaction mechanism(s) – we also inspect the PIE curves at *m/z* = 142, 143, 152, and 153 (Figs. 4 and 5). The PIE curves at *m/z* = 142 can be reproduced nicely for both systems with the 2-methylnaphthalene ($C_{11}H_{10}$) molecule; this is indicative that a methyl radical recombined with the 2-naphthyl radical followed by third body stabilization (reaction (1)). The identification of 2-ethynylnaphthalene ($C_{12}H_8$) via its molecular parent ion at *m/z* = 152 and the ^{13}C counterpart ($^{13}CC_{11}H_8$) reveals two possible pathways: the recombination of 2-naphthyl with an ethynyl radical followed by a third body stabilization (reaction (2)) or reaction of 2-naphthyl with methylacetylene to the C_3H_4-branched naphthalene intermediate ($C_{13}H_{11}^{\bullet}$) followed by methyl group loss (reaction (3)). Considering the allene reactant, the formation of 2-ethynylnaphthalene via an indirect reaction mechanism through addition to allene would require at least two successive hydrogen atom shifts in the allene moiety (4.2. Computations).

(1) $C_{10}H_7^{\bullet} + CH_3^{\bullet}$ (+M) = $C_{11}H_{10}$ (+M)

(2) $C_{10}H_7^{\bullet} + C_2H^{\bullet}$ (+M) = $C_{12}H_8$ (+M)

(3) $C_{10}H_7^{\bullet} + C_3H_4 = C_{12}H_8 + CH_3^{\bullet}$

4.2. Computations

Our work reveals that the PAHs carrying five-member rings, 1*H*-benz[*f*]indene and 3*H*-benz[*e*]indene, along with their C_3H_3-branched naphthalene isomers, can be produced via the elementary reactions of 2-naphthyl with methylacetylene/allene. To extract the underlying reaction mechanisms and the experimental data are merged with electronic structure calculations on the potential energy surfaces (PESs) (Figure 6).

4.2.1. 2-Naphthyl - Methylacetylene

The computation reveals that the 2-naphthyl radical approaches the C1 or C2 atom of methylacetylene leading to the formation of two doublet radical intermediates **[i1]** and **[i8]** through entrance barriers of 10 and 14 kJ mol^{-1}, respectively. Passing over a barrier of 22 kJ mol^{-1}, **[i1]** isomerizes to its cis-trans isomer **[i2]**, followed by a [1,2] hydrogen shift from the methyl group to the β carbon in the side chain, leading to the formation of **[i9]** followed by cis-trans isomerization to **[i10]**. The subsequent cyclization process of **[i10]** yields **[i11]**, which depicts the carbon backbone of 1*H*-benz[*f*]indene; this reaction sequence is completed by a hydrogen atom elimination producing 1*H*-benz[*f*]indene (**p1**) through a tight exit transition state in an overall exoergic reaction (-153 kJ mol^{-1}, blue line). On the other hand, **[i2]** can isomerize via cyclization to **[i3]**, ring opening to **[i4]** and cis-trans isomerization to **[i8]**. By passing over a barrier of 12 kJ mol^{-1}, intermediate **[i8]** may isomerize to **[i5];** this intermediate undergoes a [1,4] hydrogen migration from the C1 carbon of the ring to the radical position of the side chain forming **[i6]**. A second [1,4] hydrogen shift from the methyl moiety of the side chain to the *ortho* carbon of the ring leads the isomerization of **[i6]** to **[i7]**. The CH_2 moiety in the side chain approaches the C2 of the naphthalene carbon skeleton forming intermediate **[i13]**; this species carries a three-member ring, and ring opens to **[i14]**. Alternatively, through a [1,4] hydrogen shift from the C3 of naphthyl to the C=C=C moiety, **[i14]** isomerizes to **[i15]**, which undergoes cyclization step to the 1*H*-benz[*f*]indene carbon backbones in **[i17]**. A final hydrogen atom loss from the C1 carbon atom in **[i17]** leads to the formation of 1*H*-benz[*f*]indene (**p1**) by overcoming a tight exit transition state located 18 kJ mol^{-1} above the product 1*H*-benz[*f*]indene (**p1**, green line). On the other hand, a [1,4] hydrogen shift from C1 of the naphthyl moiety to the C=C=C backbone isomerizes **[i14]** to **[i16]** followed by ring closure to **[i18]**. The subsequent hydrogen emission from C1 at the five-member ring of **[i18]** yields 3*H*-benz[*e*]indene (**p2**, green line). Let us compare both routes (blue and green lines) leading to benzindene. First, 3*H*-benz[*e*]indene (**p2**) can only be produced through the

reaction sequence reactants → (**[i2]** → **[i3]** → **[i4]** →) **[i8]** → **[i5]** → **[i6]** → **[i7]** → **[i13]** → **[i14]** → **[i16]** → **[i18]** → **p2** (green line). 1*H*-benz[*f*]indene can be produced via the reaction sequence reactants → **[i2]** → **[i9]** → **[i10]** → **[i11]** → **p1** or reactants → (**[i2]** → **[i3]** → **[i4]** →) **[i8]** → **[i5]** → **[i6]** → **[i7]** → **[i13]** → **[i14]** → **[i15]** → **[i17]** → **p1** as indicated via the blue and green route, respectively. Considering the high energy transition state from **[i2]** to **[i9]** compared to **[i2]** to **[i3]**, the formation of the 1*H*-benz[*f*]indene via the sequence reactants → (**[i2]** → **[i3]** → **[i4]** →) **[i8]** → **[i5]** → **[i6]** → **[i7]** → **[i13]** → **[i14]** → **[i15]** → **[i17]** → **p1** (green pathway) should be preferred.

Except for 1*H*-benz[*f*]indene and 3*H*-benz[*e*]indene, 2-(prop-1-yn-1-yl)naphthalene (**p4**), and 2-(propa-1,2-dien-1-yl)naphthalene (**p5**) were also identified as products in 2-naphthyl – methylacetylene system. Based on the aforementioned discussion, the hydrogen loss in **[i2]** leads to the formation of 2-(prop-1-yn-1-yl)naphthalene and 2-(propa-1,2-dien-1-yl)naphthalene. Also, the [1,2] hydrogen shift in **[i2]** from the C1 to the C2 carbon of the side chain leads to **[i12]**, which may emit a hydrogen atom to generate 2-(prop-1-yn-1-yl)naphthalene (**p4**). However, the isomerization from **[i2]** to **[i12]** requires a significant barrier of 191 kJ mol^{-1} making this pathway less competitive. Moreover, 2-(prop-1-yn-1-yl)naphthalene can also be produced by the hydrogen atom loss from **[i9]**; 2-(propa-1,2-dien-1-yl)naphthalene can be generated through atomic hydrogen elimination from **[i9]** and **[i10]**. Nevertheless, due to the relatively high barrier from **[i2]** to **[i9]**, these pathways are anticipated to be less competitive. To conclude, the products **p4** and **p5** are suggested to be produced mainly from the hydrogen loss process involving intermediate **[i2]**. Besides the $C_{13}H_{10}$ products, the $C_{12}H_{10}$ product (*m/z* = 152), identified as 2-ethynylnaphthalene (**p7**), was a byproduct also observed experimentally. According to our PES calculation, it can be produced from the methyl-loss process from **[i8]** by overcoming a barrier of 143 kJ mol^{-1}.

4.2.2. 2-Naphthyl - Allene

In the 2-naphthyl – allene system, the approaching 2-naphthyl radical can add to the C1 and C2 carbons of allene leading to intermediates **[i14]** and **[i7]** by overcoming entrance barriers of 8 and 11 kJ mol^{-1}, respectively. 1*H*-benz[*f*]indene (**p1**) and 3*H*-benz[*e*]indene (**p2**) are produced, as discussed above, via the pathways color coded in green. The remaining products observed experimentally - 2-(propa-1,2-dien-1-yl)naphthalene (**p5**) and 2-(prop-2-yn-1-yl)naphthalene (**p6**) - are generated via a hydrogen loss from **[i14]** from C1 and C3 carbons on the side chain, respectively.

Note that upon formation of **[i14]**, only two isomerization steps to **[i17]** and **[i18]** are necessary prior to the decomposition to the benzindene molecules 1*H*-benz[*f*]indene (**p1**) and 3*H*-benz[*e*]indene (**p2**); four steps are required if **[i7]** is formed initially. On the other hand, the formation of benzindenes in the 2-naphthyl – methylacetylene system involves eight steps, among them intermediate **[i14]**, which efficiently links both surfaces. Therefore, **[i14]** likely presents a common intermediate in the formation of the benzindene molecule(s) in the reactions of the 2-naphthyl radical with both allene and methylacetylene. Considering that only two additional reaction steps are involved in the benzindene synthesis in the 2-naphthyl – allene system, but eight in the 2-naphthyl – methylacetylene reaction, benzindene(s) is/are preferentially formed in the reaction of 2-naphthyl radicals with allene as supported by the experimentally determined ion counts contributing to the PIE fits. Since the theoretically calculated yields of **p2** and 1*H*-benz[*e*]indene (**p3**) are very close to each other, a small photoionization cross section might explain the non-observation of the latter in both allene and methylacetylene systems. Note that the isomerization barrier of 2-naphthyl to 1-naphthyl is 251 kJ mol^{-1} [78] and the rate constant for the isomerization process at 1300 K and the pressure range typical for the reactor is 4.0×10^{3} s^{-1} corresponding to the lifetime of 250 ms, which is longer than the time the molecular beam spends in the reaction zone.[28] For the isomerization of allene to methylacetylene, it is even slower: 1.04×10^{2} s^{-1} at 1300 K. Thus, under our experiment conditions, the isomerization processes from allene to methylacetylene and from 2-naphthyl to 1-naphthyl do not happen.

4.2.3. Reaction rate constants and product branching ratios

Figure 7 shows RRKM-ME total rate constants for the reactions of 2-naphthyl with methylacetylene and allene calculated at the high-pressure (HP) and zero-pressure limits and at finite pressures (panels (a) and (d), respectively) as well as rate constants for individual bimolecular product channels at 0.03 atm characteristic inside the micro reactor (panels (b) and (e)) and in the limit of zero pressure (panels (c) and (f)) – here the calculations were actually performed at p = 10^{-10} and 10^{-15} atm, which gave nearly identical results just showing a convergence to a zero pressure. Both reactions are predicted to be relatively fast at elevated temperatures with the HP rate constants increasing from 2.1×10^{-13} to 4.1×10^{-11} cm^3 molecule cm^3 molecule^{-1} for the methylacetylene reaction and from 1.8×10^{-13} to 3.8×10^{-11} cm^3 molecule cm^3 molecule^{-1} for the allene reaction in the 500-2500 K temperature range, with the former reaction

being slightly slower than the latter. The rate constant dependence on pressure appears to be rather weak, as the fall-off behaviors begins to be observed around 800 K and at the highest considered temperature of 2500 K, the zero-pressure (and all finite-pressure) rate constants are factors of 1.6 and 2.3 lower than those at the HP limit for methylacetylene and allene, respectively. Earlier,[77] we reported RRKM-ME rate constants for the phenyl plus methylacetylene/propyne reactions, which are the prototype reactions for the growth of an extra five-member ring on a six-member ring. These rate constants are also shown for comparison in Figs. 7(a) and (d). For methylacetylene, the reaction with 2-naphthyl appears to be from a factor of 4.0 (500 K) to a factor of 2.1 (2500 K) faster than that with phenyl, whereas for allene the difference is somewhat larger, from a factor of 6.9 to 2.1 in the 500-2500 K temperature range. The difference is slightly beyond the expected accuracy for one-dimensional master equation treatment (a factor of 2) and can apparently be attributed to the fact that the entrance barriers for the 2-naphthyl + methylacetylene (10 and 14 kJ mol^{-1}) and 2-naphthyl + allene (8 and 11 kJ mol^{-1}) reactions are computed here to be a little lower than the corresponding barriers for phenyl + methylacetylene (14 and 26 kJ mol^{-1}) and phenyl + allene (11 and 15 kJ mol^{-1}). Since the differences in the barrier heights are within the expected accuracy of our G3(MP2,CC) approach, we can conclude that the rate constants for phenyl + C_3H_4 and 2-naphthyl + C_3H_4 are similar within the error bars of the present calculations. Hence, the rate constants for the prototype phenyl reactions can be used in kinetic modeling to describe a general reaction of PAH growth by a five-member ring via C_3H_4 addition to a radical site on a six-member ring, keeping in mind the rate constants may increase by factors 2-3 with the growth of the attacked aryl radical at the temperatures relevant to combustion.

The calculated rate constants for individual product channels and product branching ratios presented in Table S1 in ESI show a strong temperature and pressure dependence. At $p = 0.03$ atm characteristic for the micro reactor conditions, the three-ring products **p1**, **p2**, and **p3** are predicted to be preferably formed among bimolecular products in the reaction of 2-naphthyl with allene up to the temperature of 1200 K. In the meantime, at low temperatures, up to 1100 K, collisional stabilization of the $C_{13}H_{11}$ intermediates **[i14]** and **[i7]** is favored over the formation of the bimolecular products. Above 1200 K, the formation of the two-ring-side-chain products, especially **p6** (27-82%), followed by **p7** (10-11% to 5%) and **p5** (5-8%) takes over and represents most preferable reaction channels. Nevertheless, at 1300 K, which is the highest temperature in the micro reactor in the present work, the predicted relative yields of **p1**, **p2**, and **p3** – 16.5%, 9.4%,

and 9.3%, respectively, are still significant. Alternatively, the reaction of 2-naphthyl with methylacetylene is calculated to have a lower tendency to form the three-ring products. Here, the collisional stabilization of $C_{13}H_{11}$, mostly **[i1]**, dominates the reaction below 800 K and at higher temperatures the main product is **p4** (26-61%) followed by **p7** (12-31%) and **p5** (3-7%). The overall calculated yield of the three-ring products **p1-p3** is 0.77% at 1300 K and it further decreases with temperature. The RRKM-ME calculation results are in qualitative agreement with experiment except of the non-observation of **p3**, which is predicted to have a similar branching ratio to that of **p2**. In the meantime, a direct quantitative comparison between theory and experiment is not warranted for several reasons. First, the absolute photoionization cross sections of the product isomers are unknown. Second, the temperature and pressure distribution inside the micro reactor is not uniform and hence, the reaction takes place under different conditions as the molecules traverse the reactor. Third, there is sufficient time for secondary reactions to occur; in particular, the more thermodynamically favorable three-ring products can be produced via secondary H-assisted isomerization of **p4-p6** products similar to how indene can be formed via H-assisted isomerization of the primary *c*-C_6H_5-C_3H_3 ring-side-chain products of the C_6H_5 + C_3H_4 reaction.[77]

Theoretical calculations allow us to predict how the reaction outcome would change under different pressures. For instance, while considering p = 1 atm typical for combustion, we find that the collisional stabilization of the $C_{13}H_{11}$ complexes prevails up to higher temperatures, 1300 and 1000 K for the allene and methylacetylene reactions, respectively. At higher temperatures, the formation of the two-ring-side-chain products is preferable (**p6** followed by **p5** and **p7** for allene and **p4** followed by **p7** and **p5** for methylacetylene). At the typical combustion temperature of 1500 K, the calculated total yield of **p1-p3** is about 19% for allene and only ~0.2% for methylacetylene, with **p1** being somewhat more preferable product than **p2** and **p3**. The decrease of pressure, on the contrary, should increase the yield of the three-ring aromatic products, mostly because they are favored enthalpically and are disfavored entropically and the collisional stabilization of $C_{13}H_{11}$ becomes less and less probable as the pressure drops. In the limit of zero-pressure, where only radiational stabilization of $C_{13}H_{11}$ is possible, the formation of **p1-p3** prevails in the 2-naphthyl + allene reaction in the temperature range of 300-1200 K and in the 2-naphthyl + methylacetylene reaction in the range of 300-500 K (Table S1). Although the reactions exhibits entrance barriers and are not realistic in molecular clouds at temperatures about 10 K, they would be feasible at the temperatures characteristic for circumstellar envelopes of carbon rich AGB stars,

with the rate constants being in the range of $1.9\times10^{-14} - 5.0\times10^{-12}$ (allene) and $1.6\times10^{-14} - 7.4\times10^{-12}$ (methylacetylene) cm^3 $molecule^{-1}$ s^{-1} at T = 300-1500 K. Since the formation of the three-ring aromatic products is favored at very low pressures, the reactions of 2-naphthyl with the C_3H_4 isomers may play a more important role in the PAH growth in circumstellar envelopes than in combustion on Earth.

It should be noted that in combustion systems, molecular mass growth processes are counterbalanced by degradation of PAH radicals by molecular oxygen as demonstrated in the phenyl – molecular oxygen system.[79-81] Here, anthracenyl and/or phenanthrenyl radical reactions with molecular oxygen could also lead via ring contraction of a six-membered ring to a five-membered ring forming benzindenes. In the combustion of coal, the amount of indene benzologues increased with the oxygen concentration. Wornat et al. stated that benz[*f*]indene could be formed via molecular oxygen addition to the 1- or 2-anthryl radical, followed by carbon monoxide elimination and hydrogen loss (Scheme 6).[82] This oxy radical pathway could dominate above 900 K as analogous to the reaction of phenyl plus molecular oxygen.[83, 84] Similarly, phenanthrenyl radicals can also lead to $C_{13}H_{10}$ isomers (Scheme 7). Moreover, Norinaga et al.[85, 86] proposed the mechanism for benz[*f*]indene formation from pyrolysis of unsaturated light hydrocarbons, however, recent experiments in our laboratory could not support this conclusion.[87]

5. Conclusion

Our combined experimental and computational studies revealed critical mass growth processes involving the addition of a five-membered ring to an aromatic aryl radical (2-naphthyl) leading to two distinct three-membered ring PAHs carrying two six- and one five-membered ring: 3*H*-benz[*e*]indene and 1*H*-benz[*f*]indene. The underlying reaction mechanisms involve the initial addition of the 2-naphthyl radical with its radical center to the π-electron density of the allene and methylacetylene reactants through entrance barriers between 8-11 and 10-14 kJ mol^{-1}, followed by extensive isomerization (hydrogen shifts, ring closure), and termination via atomic hydrogen losses accompanied by aromatization in overall exoergic reaction with both surfaces connected via intermediate **[i14]**. The reaction mechanisms essentially mirror the formation of the indene molecule (C_9H_8) in the phenyl-allene and phenyl-methylacetylene systems[9, 88, 89] and suggest that the second aromatic ring in the 2-naphthyl radical acts as a spectator. These findings propose that if in a polycyclic aromatic hydrocarbon, hydrogen abstraction from a six-membered ring leads to

a PAH radical, this radical can react with allene or methylacetylene through ring annulation. Based on electronic structure calculations, Mebel et al.[77] et al. predicted that once PAHs carrying a five-membered ring lose a hydrogen atom from the latter, the cyclopentadienyl radical moiety may react with a methyl radical (CH_3) through ring expansion leading eventually to a six-membered ring (Scheme 5). Therefore, the mass growth via the methylacetylene/allene reaction with aryl radicals leading first via ring annulation to a 5-membered ring followed by methyl radical induced ring expansion may represent a strong alternative to ring annulation of aryl radicals via HACA through reaction with two acetylene molecules in high temperature environments.

Acknowledgments

This work was supported by the US Department of Energy, Basic Energy Sciences DE-FG02-03ER15411 (experimental studies) and DE-FG02-04ER15570 (computational studies; synthesis of the $C_{13}H_{10}$ isomers) to the University of Hawaii (UH) and Florida International University (FIU), respectively. U.A., W.L., B.X., and M.A. are supported by the Director, Office of Science, Office of Basic Energy Sciences, of the U.S. Department of Energy under Contract No. DE-AC02-05CH11231, through the Gas Phase Chemical Physics program of the Chemical Sciences Division. The ALS is supported under the same contract. Ab initio and RRKM-ME calculations at Samara University were supported by the Ministry of Higher Education and Science of the Russian Federation under Grant No. 14.Y26.31.0020. A.D.O. also thanks the Ministry of Higher Education and Science of the Russian Federation for his Presidential Scholarship to stay at FIU in the Spring Semester 2019. A.H.H. acknowledges support from FIU for a Presidential Fellowship.

Author Contributions

R.I.K. designed the experiment; L.Z., M.P., B.X., U.A. and W.L. carried out the experimental measurements; M.A. supervised the experiment; L.Z. performed the data analysis; A.D.O., V.N.A. and A.M.M. carried out the theoretical analysis; A.H.H. and S.F.W. synthesized the compounds, A.M.M., and M.A. discussed the data; R.I.K., A.M.M. and L.Z. wrote the manuscript.

References

1. R. I. Kaiser, *Chem. Rev.*, 2002, **102**, 1309-1358.
2. R. I. Kaiser and N. Balucani, *Acc. Chem. Res.*, 2001, **34**, 699-706.
3. K. Liu, *Annu. Rev. Phys. Chem.*, 2001, **52**, 139-164.
4. X. Yang and D. H. Zhang, *Acc. Chem. Res.*, 2008, **41**, 981-989.
5. B. Joalland, Y. Shi, A. D. Estillore, A. Kamasah, A. M. Mebel and A. G. Suits, *J. Phys. Chem. A*, 2014, **118**, 9281-9295.
6. F. T. Zhang, R. I. Kaiser, A. Golan, M. Ahmed and N. Hansen, *J. Phys. Chem. A*, 2012, **116**, 3541-3546.
7. A. Golan, M. Ahmed, A. M. Mebel and R. I. Kaiser, *Phys. Chem. Chem. Phys.*, 2013, **15**, 341-347.
8. K. N. Urness, Q. Guan, A. Golan, J. W. Daily, M. R. Nimlos, J. F. Stanton, M. Ahmed and G. B. Ellison, *J. Chem. Phys.*, 2013, **139**, 124305.
9. F. Zhang, R. I. Kaiser, V. V. Kislov, A. M. Mebel, A. Golan and M. Ahmed, *J. Phys. Chem. Lett.*, 2011, **2**, 1731-1735.
10. A. G. G. M. Tielens, *Annu. Rev. Astron. Astr.*, 2008, **46**, 289-337.
11. A. G. G. M. Tielens, *Rev. Mod. Phys.*, 2013, **85**, 1021-1081.
12. A. G. G. M. Tielens and L. J. Allamandola, Cool Interstellar Physics and Chemistry, 2011.
13. A. G. G. M. Tielens, *EAS Publ. Ser.*, 2009, **35**, 33-56.
14. E. Peeters, L. J. Allamandola, D. M. Hudgins, S. Hony and A. G. G. M. Tielens, *Astron. Soc. Pac. Conf. Ser.*, 2004, **309**, 141-162.
15. A. G. G. M. Tielens and E. Peeters, *Springer Proc. Phys.*, 2004, **91**, 497-506.
16. L. J. Allamandola, *EAS Publ. Ser.*, 2011, **46**, 305-317.
17. L. J. Allamandola, *ACS Symp. Ser.*, 2007, **981**, 80-110.
18. L. Biennier, F. Salama, L. J. Allamandola, J. J. Scherer and A. O'Keefe, *NASA Conf. Publ.*, 2002, **2002-211863**, 113-116.
19. L. J. Allamandola and D. M. Hudgins, *NATO Sci. Ser., II*, 2003, **120**, 251-316.
20. Y. Liu, M. Junaid, N. Hamid, C.-D. Chen and D.-S. Pei, *Am. J. Environ. Sci.*, 2018, **14**, 129-155.
21. O. Idowu, K. T. Semple, K. Ramadass, W. O'Connor, P. Hansbro and P. Thavamani, *Environ. Int.*, 2019, **123**, 543-557.
22. M. Oliveira, K. Slezakova, C. Delerue-Matos, M. C. Pereira and S. Morais, *Environ. Int.*, 2019, **124**, 180-204.
23. S. Gitipour, G. A. Sorial, S. Ghasemi and M. Bazyari, *Environ. Monit. Assess.*, 2018, **190**, 1-17.
24. A. M. Mebel, V. V. Kislov and R. I. Kaiser, *J. Am. Chem. Soc.*, 2008, **130**, 13618-13629.
25. M. Frenklach and H. Wang, *Proc. Combust. Inst.*, 1991, **23**, 1559-1566.
26. M. Frenklach and E. D. Feigelson, *Astrophys. J.*, 1989, **341**, 372-384.
27. L. Zhao, R. I. Kaiser, B. Xu, U. Ablikim, M. Ahmed, M. M. Evseev, E. K. Bashkirov, V. N. Azyazov and A. M. Mebel, *Nat. Astron.*, 2018, **2**, 973-979.
28. L. Zhao, R. I. Kaiser, B. Xu, U. Ablikim, M. Ahmed, M. V. Zagidullin, V. N. Azyazov, A. H. Howlader, S. F. Wnuk and A. M. Mebel, *J. Phys. Chem. Lett.*, 2018, **9**, 2620-2626.
29. L. Zhao, B. Xu, U. Ablikim, W. Lu, M. Ahmed, M. M. Evseev, E. K. Bashkirov, V. N. Azyazov, A. H. Howlader, S. F. Wnuk, A. M. Mebel and R. I. Kaiser, *ChemPhysChem*, 2019, **20**, 791-797.

30. A. M. Mebel, A. Landera and R. I. Kaiser, *J. Phys. Chem. A*, 2017, **121**, 901-926.
31. L. Zhao, R. I. Kaiser, B. Xu, U. Ablikim, M. Ahmed, D. Joshi, G. Veber, F. R. Fischer and A. M. Mebel, *Nat. Astron.*, 2018, **2**, 413-419.
32. H. Wang and M. Frenklach, *J. Phys. Chem.*, 1994, **98**, 11465-11489.
33. D. S. Parker, F. Zhang, Y. S. Kim, R. I. Kaiser, A. Landera, V. V. Kislov, A. M. Mebel and A. Tielens, *Proc. Natl. Acad. Sci. U.S.A.*, 2012, **109**, 53-58.
34. A. E. Karataş and Ö. L. Gülder, *Prog. Energy Combust. Sci.*, 2012, **38**, 818-845.
35. D. S. Parker, R. I. Kaiser, O. Kostko and M. Ahmed, *ChemPhysChem*, 2015, **16**, 2091-2093.
36. T. Yang, D. S. N. Parker, B. B. Dangi, R. I. Kaiser and A. M. Mebel, *Phys. Chem. Chem. Phys.*, 2015, **17**, 10510-10519.
37. L. Vereecken, H. F. Bettinger and J. Peeters, *Phys. Chem. Chem. Phys.*, 2002, **4**, 2019-2027.
38. L. Vereecken, J. Peeters, H. F. Bettinger, R. I. Kaiser, P. v. R. Schleyer and H. F. Schaefer, III, *J. Am. Chem. Soc.*, 2002, **124**, 2781-2789.
39. D. D. S. Parker, D. F. Zhang, D. R. I. Kaiser, D. V. V. Kislov and D. A. M. Mebel, *Chemistry–An Asian Journal*, 2011, **6**, 3035-3047.
40. D. S. N. Parker, R. I. Kaiser, B. Bandyopadhyay, O. Kostko, T. P. Troy and M. Ahmed, *Angew. Chem. Int. Ed.*, 2015, **54**, 5421-5424.
41. Y. Li, L. Zhang, T. Yuan, K. Zhang, J. Yang, B. Yang, F. Qi and C. K. Law, *Combust. Flame*, 2010, **157**, 143-154.
42. T. Zhang, L. Zhang, X. Hong, K. Zhang, F. Qi, C. K. Law, T. Ye, P. Zhao and Y. Chen, *Combust. Flame*, 2009, **156**, 2071-2083.
43. W. Yuan, Y. Li, P. Dagaut, J. Yang and F. Qi, *Combust. Flame*, 2015, **162**, 3-21.
44. H. Richter, W. J. Grieco and J. B. Howard, *Combust. Flame*, 1999, **119**, 1-22.
45. H. Richter, O. A. Mazyar, R. Sumathi, W. H. Green, J. B. Howard and J. W. Bozzelli, *J. Phys. Chem. A*, 2001, **105**, 1561-1573.
46. N. Olten and S. Senkan, *Combust. Flame*, 1999, **118**, 500-507.
47. A. Kitajima, T. Hatanaka, M. Takeuchi, H. Torikai and T. Miyadera, *Combust. Flame*, 2005, **142**, 72-88.
48. C. S. McEnally and L. D. Pfefferle, *Combust. Flame*, 2007, **148**, 210-222.
49. V. Kislov and A. Mebel, *J. Phys. Chem. A*, 2008, **112**, 700-716.
50. L. Vereecken and J. Peeters, *Phys. Chem. Chem. Phys.*, 2003, **5**, 2807-2817.
51. J. Bittner and J. Howard, *Proc. Combust. Inst.*, 1981, **18**, 1105-1116.
52. J. DeCoster, A. Ergut, Y. A. Levendis, H. Richter, J. B. Howard and J. B. Carlson, *Proc. Combust. Inst.*, 2007, **31**, 491-499.
53. F. Zhang, X. Gu and R. I. Kaiser, *J. Chem. Phys.*, 2008, **128**, 084315.
54. R. Sivaramakrishnan, R. S. Tranter and K. Brezinsky, *J. Phys. Chem. A*, 2006, **110**, 9400-9404.
55. M. Frenklach, D. W. Clary, W. C. Gardiner Jr and S. E. Stein, *Proc. Combust. Inst.*, 1988, **21**, 1067-1076.
56. M. Frenklach, T. Yuan and M. Ramachandra, *Energy Fuels*, 1988, **2**, 462-480.
57. V. Kislov and A. Mebel, *J. Phys. Chem. A*, 2007, **111**, 3922-3931.
58. T. R. Melton, A. M. Vincitore and S. M. Senkan, *Proc. Combust. Inst.*, 1998, **27**, 1631-1637.
59. T. R. Melton, F. Inal and S. M. Senkan, *Combust. Flame*, 2000, **121**, 671-678.

60. Y. Li, L. Zhang, Z. Tian, T. Yuan, K. Zhang, B. Yang and F. Qi, *Proc. Combust. Inst.*, 2009, **32**, 1293-1300.
61. M. Kamphus, M. Braun-Unkhoff and K. Kohse-Höinghaus, *Combust. Flame*, 2008, **152**, 28-59.
62. N. M. Marinov, W. J. Pitz, C. K. Westbrook, A. M. Vincitore, M. J. Castaldi, S. M. Senkan and C. F. Melius, *Combust. Flame*, 1998, **114**, 192-213.
63. J. J. Newby, J. A. Stearns, C.-P. Liu and T. S. Zwier, *J. Phys. Chem. A*, 2007, **111**, 10914-10927.
64. B. Yang, Y. Li, L. Wei, C. Huang, J. Wang, Z. Tian, R. Yang, L. Sheng, Y. Zhang and F. Qi, *Proc. Combust. Inst.*, 2007, **31**, 555-563.
65. Y. Li, L. Zhang, Z. Tian, T. Yuan, J. Wang, B. Yang and F. Qi, *Energy Fuels*, 2009, **23**, 1473-1485.
66. G. da Silva and J. W. Bozzelli, *J. Phys. Chem. A*, 2009, **113**, 6979-6986.
67. D. H. Kim, J. A. Mulholland, D. Wang and A. Violi, *J. Phys. Chem. A*, 2010, **114**, 12411-12416.
68. A. Lamprecht, B. Atakan and K. Kohse-Höinghaus, *Proc. Combust. Inst.*, 2000, **28**, 1817-1824.
69. F. Qi, *Proc. Combust. Inst.*, 2013, **34**, 33-63.
70. L. A. Curtiss, K. Raghavachari, P. C. Redfern, V. Rassolov and J. A. Pople, *J. Chem. Phys.*, 1998, **109**, 7764-7776.
71. L. A. Curtiss, K. Raghavachari, P. C. Redfern, A. G. Baboul and J. A. Pople, *Chem. Phys. Lett.*, 1999, **314**, 101-107.
72. A. G. Baboul, L. A. Curtiss, P. C. Redfern and K. Raghavachari, *J. Chem. Phys.*, 1999, **110**, 7650-7657.
73. M. J. Frisch, G. W. Trucks, H. B. Schlegel, G. E. Scuseria, M. A. Robb, J. R. Cheeseman, G. Scalmani, V. Barone, B. Mennucci, G. A. Petersson, H. Nakatsuji, M. Caricato, X. Li, H. P. Hratchian, A. F. Izmaylov, J. Bloino, G. Zheng, J. L. Sonnenberg, M. Hada, M. Ehara, K. Toyota, R. Fukuda, J. Hasegawa, M. Ishida, T. Nakajima, Y. Honda, O. Kitao, H. Nakai, T. Vreven, J. A. Montgomery, Jr., J. E. Peralta, F. Ogliaro, M. Bearpark, J. J. Heyd, E. Brothers, K. N. Kudin, V. N. Staroverov, T. Keith, R. Kobayashi, J. Normand, K. Raghavachari, A. Rendell, J. C. Burant, S. S. Iyengar, J. Tomasi, M. Cossi, N. Rega, J. M. Millam, M. Klene, J. E. Knox, J. B. Cross, V. Bakken, C. Adamo, J. Jaramillo, R. Gomperts, R. E. Stratmann, O. Yazyev, A. J. Austin, R. Cammi, C. Pomelli, J. W. Ochterski, R. L. Martin, K. Morokuma, V. G. Zakrzewski, G. A. Voth, P. Salvador, J. J. Dannenberg, S. Dapprich, A. D. Daniels, O. Farkas, J. B. Foresman, J. V. Ortiz, J. Cioslowski and D. J. Fox, Gaussian 09, revision A.02, (Gaussian Inc., CT), 2009.
74. H. J. Werner, P. J. Knowles, G. Knizia, F. R. Manby, M. Schütz, P. Celani, W. Györffy, D. Kats, T. Korona, R. Lindh, A. Mitrushenkov, G. Rauhut, K. R. Shamasundar, T. B. Adler, R. D. Amos, A. Bernhardsson, A. Berning, D. L. Cooper, M. J. O. Deegan, A. J. Dobbyn, F. Eckert, E. Goll, C. Hampel, A. Hesselmann, G. Hetzer, T. Hrenar, G. Jansen, C. Köppl, Y. Liu, A. W. Lloyd, R. A. Mata, A. J. May, S. J. McNicholas, W. Meyer, M. E. Mura, A. Nicklaß, D. P. O'Neill, P. Palmieri, D. Peng, K. Pflüger, R. Pitzer, M. Reiher, T. Shiozaki, H. Stoll, A. J. Stone, R. Tarroni, T. Thorsteinsson and M. Wang, MOLPRO, version 2010.1, http://www.molpro.net, (University College Cardiff Consultants Ltd, United Kingdom), 2010.

75. Y. Georgievskii, J. A. Miller, M. P. Burke and S. J. Klippenstein, *J. Phys. Chem. A*, 2013, **117**, 12146-12154.
76. Y. Georgievskii and S. J. Klippenstein, *MESS Program Package,* http://tcg.cse.anl.gov/papr, 2015.
77. A. M. Mebel, Y. Georgievskii, A. W. Jasper and S. J. Klippenstein, *Faraday Discuss.*, 2016, **195**, 637-670.
78. A. M. Mebel, Y. Georgievskii, A. W. Jasper and S. J. Klippenstein, *Proc. Combust. Inst.*, 2017, **36**, 919-926.
79. D. S. Parker, R. I. Kaiser, T. P. Troy, O. Kostko, M. Ahmed and A. M. Mebel, *J. Phys. Chem. A*, 2014, **119**, 7145-7154.
80. X. Gu, F. Zhang and R. I. Kaiser, *Chem. Phys. Lett.*, 2007, **448**, 7-10.
81. D. S. Parker, F. Zhang and R. I. Kaiser, *J. Phys. Chem. A*, 2011, **115**, 11515-11518.
82. M. J. Wornat, C. J. Mikolajczak, B. A. Vernaglia and M. A. Kalish, *Energy Fuels*, 1999, **13**, 1092-1096.
83. I. V. Tokmakov, G.-S. Kim, V. V. Kislov, A. M. Mebel and M. C. Lin, *J. Phys. Chem. A*, 2005, **109**, 6114-6127.
84. N. Sebbar, H. Bockhorn and J. Bozzelli, *Int. J. Chem. Kinet.*, 2008, **40**, 583-604.
85. K. Norinaga, O. Deutschmann, N. Saegusa and J.-i. Hayashi, *J. Anal. Appl. Pyrolysis*, 2009, **86**, 148-160.
86. G. Badger, S. Jolad and T. Spotswood, *Aust. J. Chem.*, 1966, **19**, 95-105.
87. L. Zhao, M. B. Prendergast, R. I. Kaiser, B. Xu, W. Lu, U. Ablikim, M. Ahmed, A. D. Oleinikov, V. N. Azyazov, A. M. Mebel, A. H. Howlader and S. F. Wnuk, *ChemPhysChem*, 2019, doi:10.1002/cphc.201900052.
88. R. Kaiser, L. Vereecken, J. Peeters, H. Bettinger, P. v. R. Schleyer and H. Schaefer, *A & A*, 2003, **406**, 385-392.
89. X. Gu and R. I. Kaiser, *Acc. Chem. Res.*, 2008, **42**, 290-302.

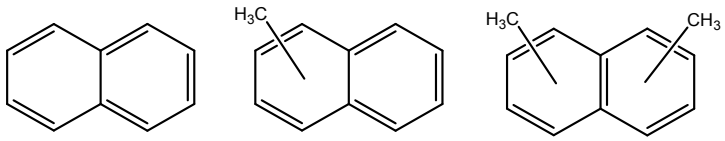

Scheme 1: Prototype polycyclic aromatic hydrocarbon naphthalene together with (di)methyl substituted counterparts formed in the reactions of phenyl-type radicals (phenyl, tolyl).

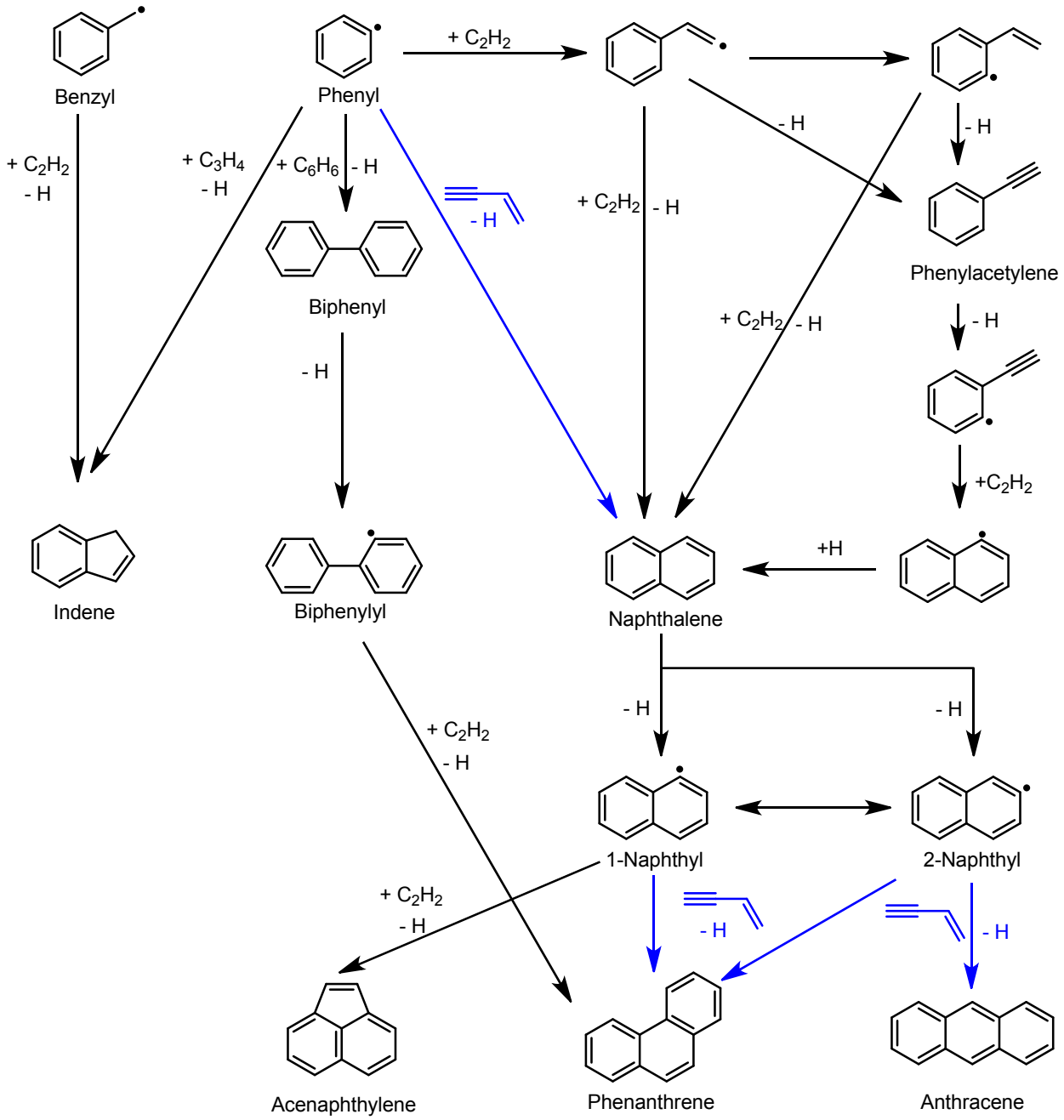

Scheme 2: Experimentally verified possible mass growth processes to bi- and tricyclic PAHs via the hydrogen abstraction – acetylene addition (HACA) (black) and the barrier-less hydrogen abstraction – vinylacetylene addition (HAVA) pathways (blue). Note that biphenyl is formed via hydrogen abstraction – phenyl addition.

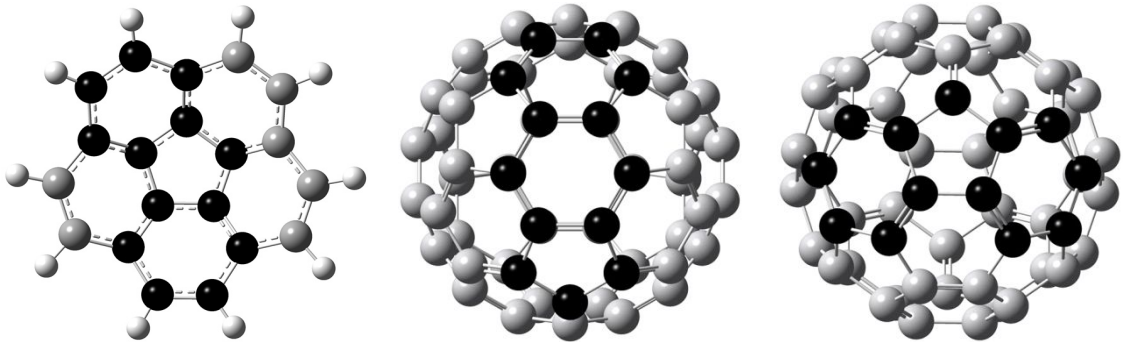

Scheme 3: The role of fluorene and benzindene backbones (black) as building blocks of corannulene (left) and fullerenes (center, right).

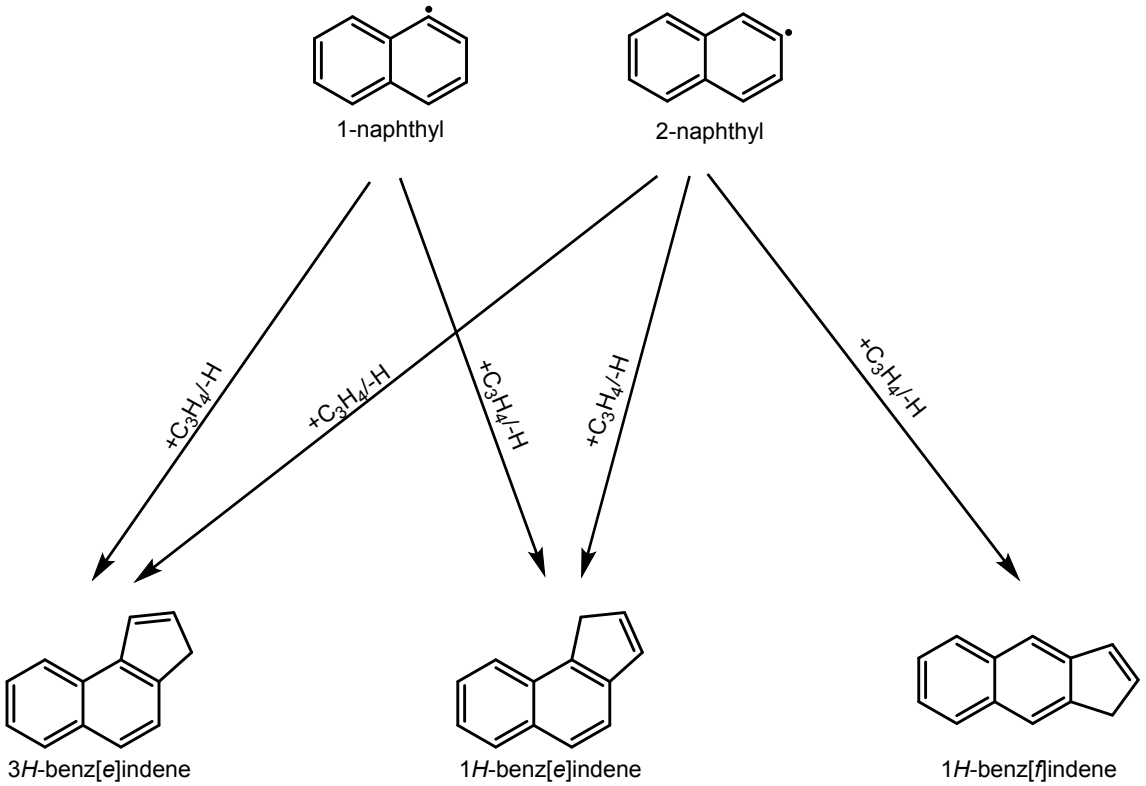

Scheme 4: Proposed stepwise formation of prototype tricyclic PAHs carrying a single five-membered ring. In combustion flames, naphthyl radicals are generated via unimolecular decomposition of or via hydrogen abstraction from naphthalene.

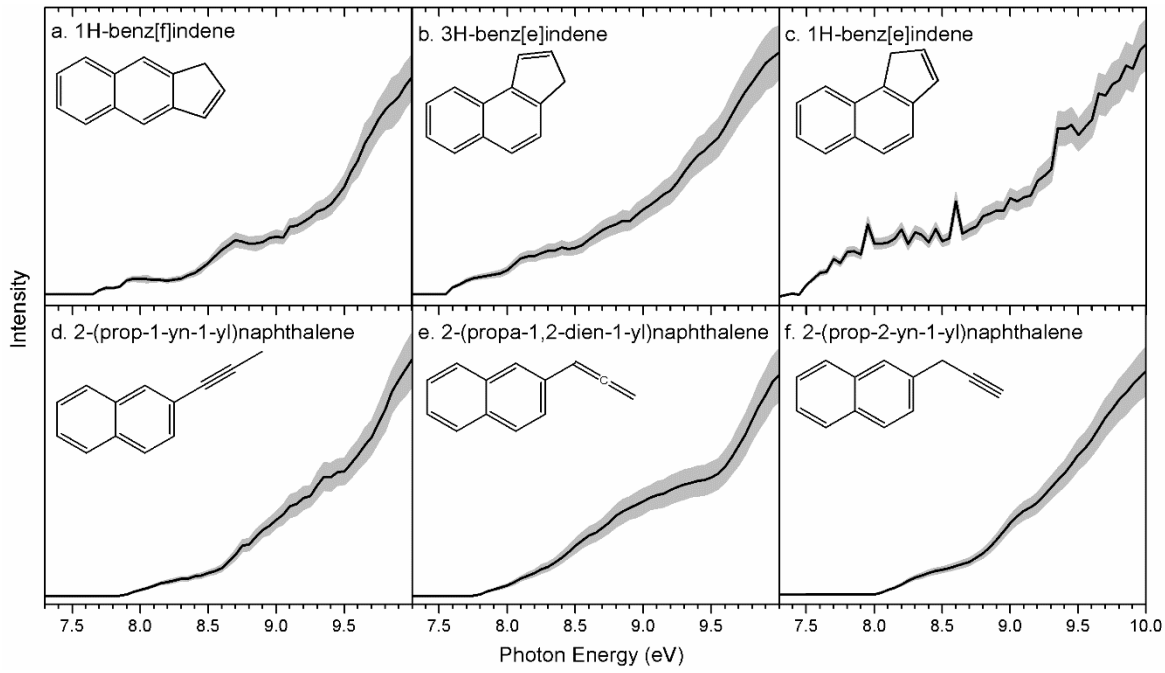

Figure 1. PIE calibration curves for distinct $C_{13}H_{10}$ isomers: 1*H*-benz[*f*]indene (**p1**; 7.75 ± 0.05 eV), 3*H*-benz[*e*]indene (**p2**; 7.55 ± 0.05 eV), 1*H*-benz[*e*]indene (**p3**; 7.45 ± 0.05 eV), 2-(prop-1-yn-1-yl)naphthalene (**p4**; 7.85 ± 0.05 eV), 2-(propa-1,2-dien-1-yl)naphthalene (**p5**; 7.75 ± 0.05 eV) and 2-(prop-2-yn-1-yl)naphthalene (**p6**; 8.00 ± 0.05 eV). The values in the parenthesis indicates the ionization energies. The overall error bars (grey area) consist of two parts: ±10% based on the accuracy of the photodiode and a 1 σ error of the PIE curve averaged over the individual scans.

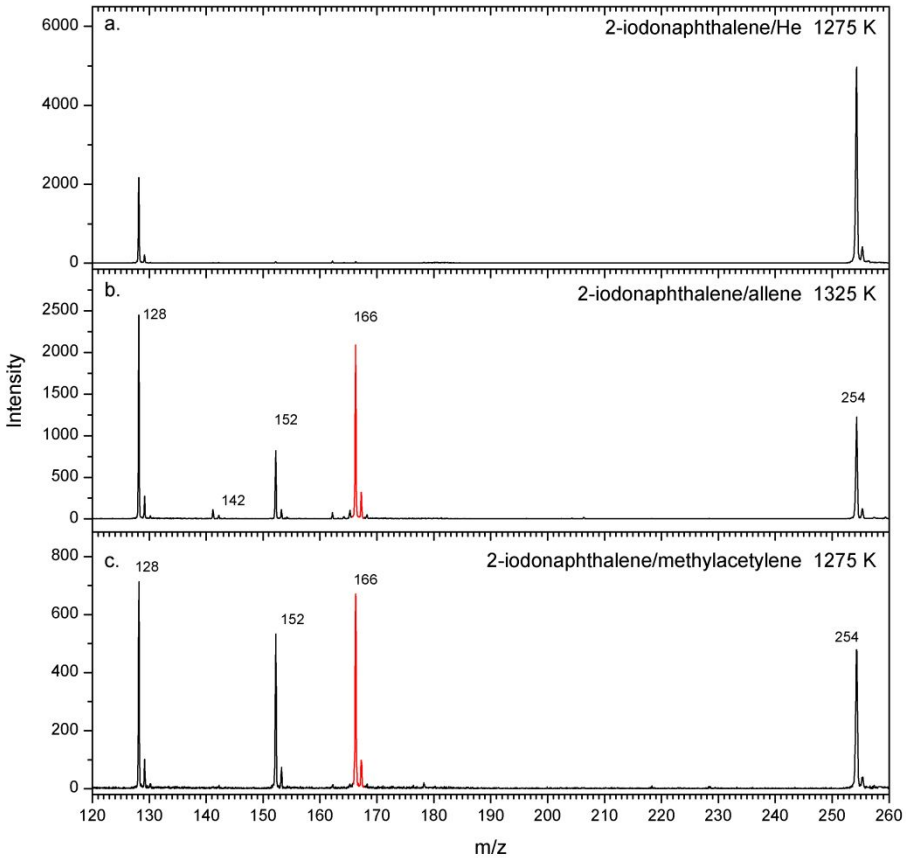

Figure 2. Comparison of photoionization mass spectra recorded at a photon energy of 9.50 eV and various reactor temperatures. (a) 2-iodonaphthalene ($C_{10}H_7I$) - helium (He) system at 1275 K; (b) 2-iodonaphthalene ($C_{10}H_7I$) - allene (C_3H_4) system at 1325 K; and (c) 2-iodonaphthalene ($C_{10}H_7I$) - methylacetylene (C_3H_4) system at 1275 K. The mass peaks of the newly formed $C_{13}H_{10}$ (*m/z* = 166) species along with the ^{13}C-counterparts (*m/z* = 167) are highlighted in red.

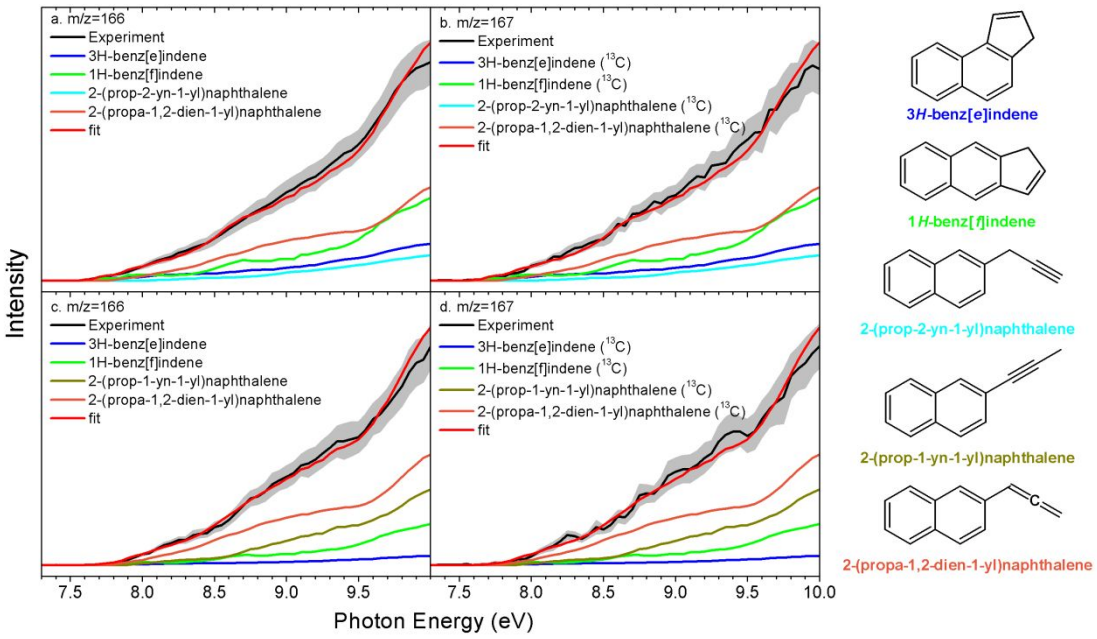

Figure 3. Photoionization efficiency (PIE) curves for reaction systems of (a) and (b): 2-naphthyl ($C_{10}H_7^{\bullet}$) + allene (C_3H_4); (c) and (d): 2-naphthyl ($C_{10}H_7^{\bullet}$) + methylacetylene (C_3H_4). Black: experimentally derived PIE curves; colored lines (green, blue, purple and dark yellow): reference PIE curves; red lines: overall fit. The overall error bars consist of two parts: ±10% based on the accuracy of the photodiode and a 1 σ error of the PIE curve averaged over the individual scans.

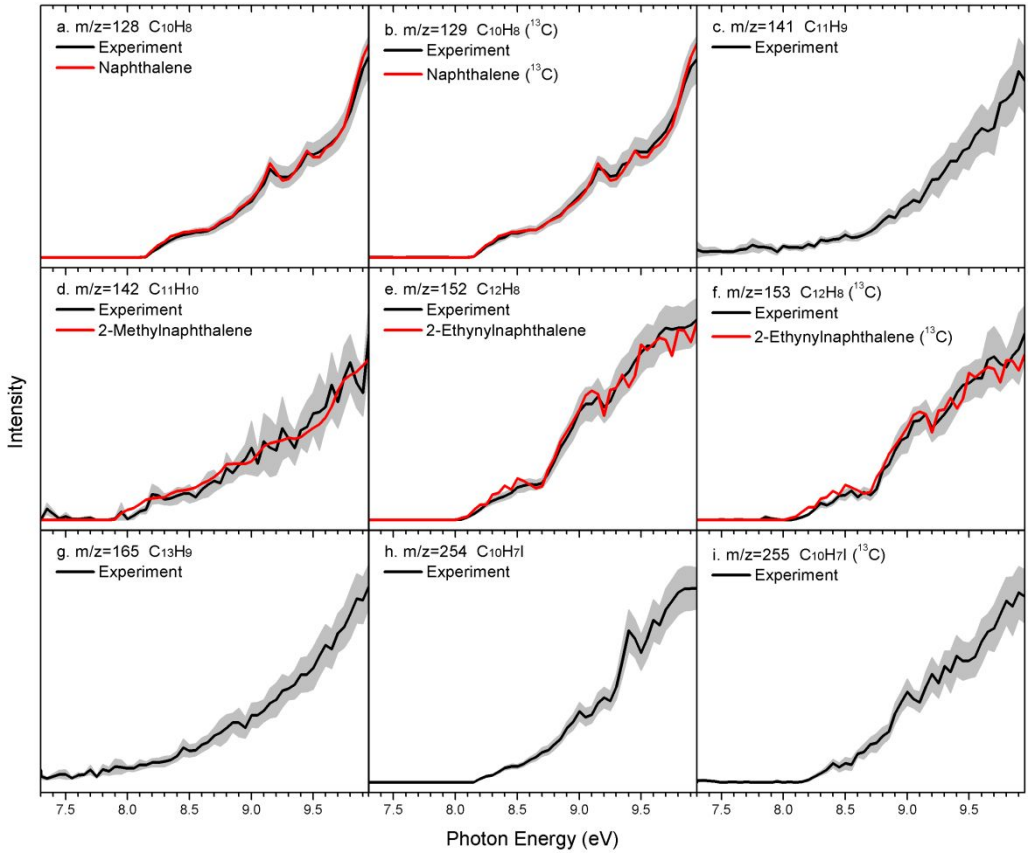

Figure 4. Photoionization efficiency (PIE) curves in the reaction of 2-naphthyl ($C_{10}H_7^{\bullet}$) and allene (C_3H_4) along with the experimental errors (gray area) and the reference PIE curves (red lines). In the high temperature condition, methyl (CH_3) is produced in the pyrolysis process, reacting with 2-naphthyl radical to produce 2-methylnaphthalene (*m/z* = 142). Moreover, 2-methylnaphthalene will loss a hydrogen atom to yield a radical with the resonantly-stabilized structure (*m/z* = 141). Acetylene is also one of major small products formed in the pyrolysis. It can add to 2-naphthyl radical followed by H-loss to form 2-ethynylnaphthalene (*m/z* = 152). Besides, 2-ethynylnaphthalene can also be produced from the CH_3-loss from intermediate **[i8]** by overcoming a barrier of 143 kJ mol^{-1}. Product at *m/z* = 165 may be the H-loss product from 1*H*-benz[*f*]indene and 3*H*-benz[*e*]indene. It is also a resonantly-stabilized species. Species at *m/z* = 254 and 255 are the precursor and the ^{13}C counterparts.

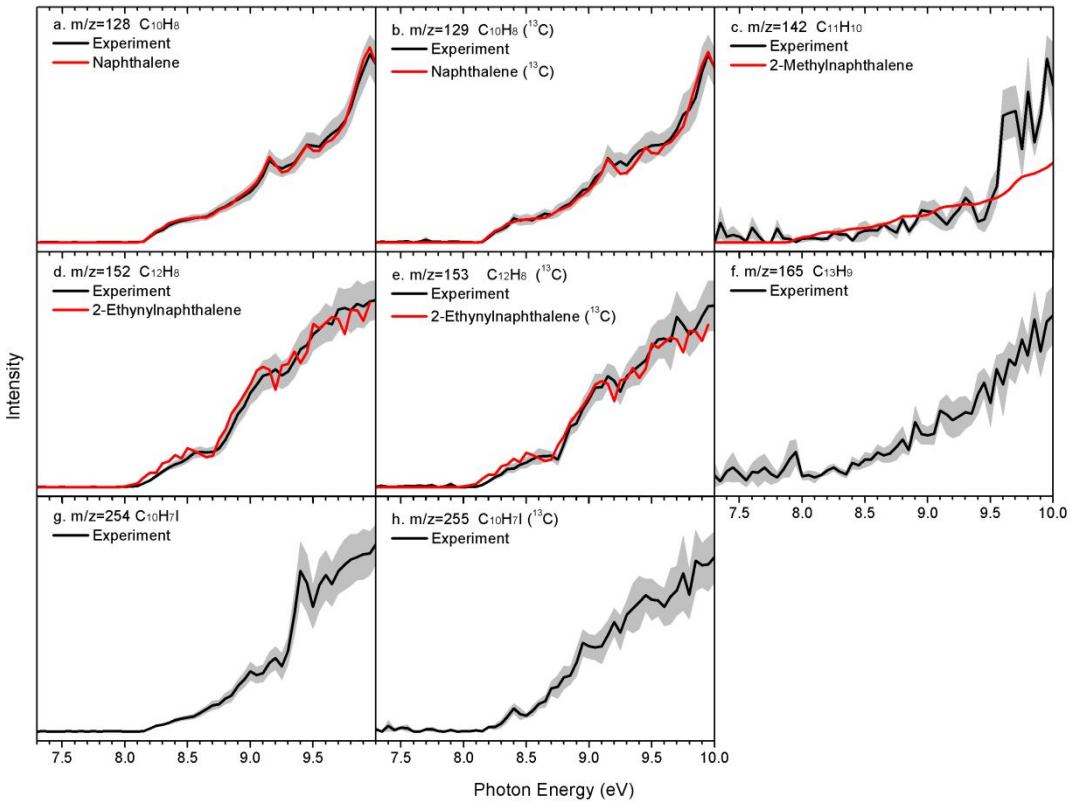

Figure 5. Photoionization efficiency (PIE) curves in the reaction of 2-naphthyl ($C_{10}H_7^{\bullet}$) and methylacetylene (C_3H_4) along with the experimental errors (gray area) and the reference PIE curves (red lines). In the high temperature condition, methyl (CH_3) is produced in the pyrolysis process, reacting with 2-naphthyl radical to produce 2-methylnaphthalene (*m/z* = 142). Due to the low production at *m/z* =142, the PIE curve is relatively worse compared with that in 2-naphthyl – allene system. Acetylene is one of major small products formed in the pyrolysis. It can add to 2-naphthyl radical followed by H-loss to form 2-ethynylnaphthalene (*m/z* = 152). Besides, 2-ethynylnaphthalene can also be produced from the CH_3-loss from intermediate **[i8]** by overcoming a barrier of 143 kJ mol^{-1}. Product at *m/z* = 165 may be the H-loss products from 1*H*-benz[*f*]indene and 3*H*-benz[*e*]indene. It is also a resonantly-stabilized species. Species at *m/z* = 254 and 255 are the precursor and the ^{13}C counterpart.

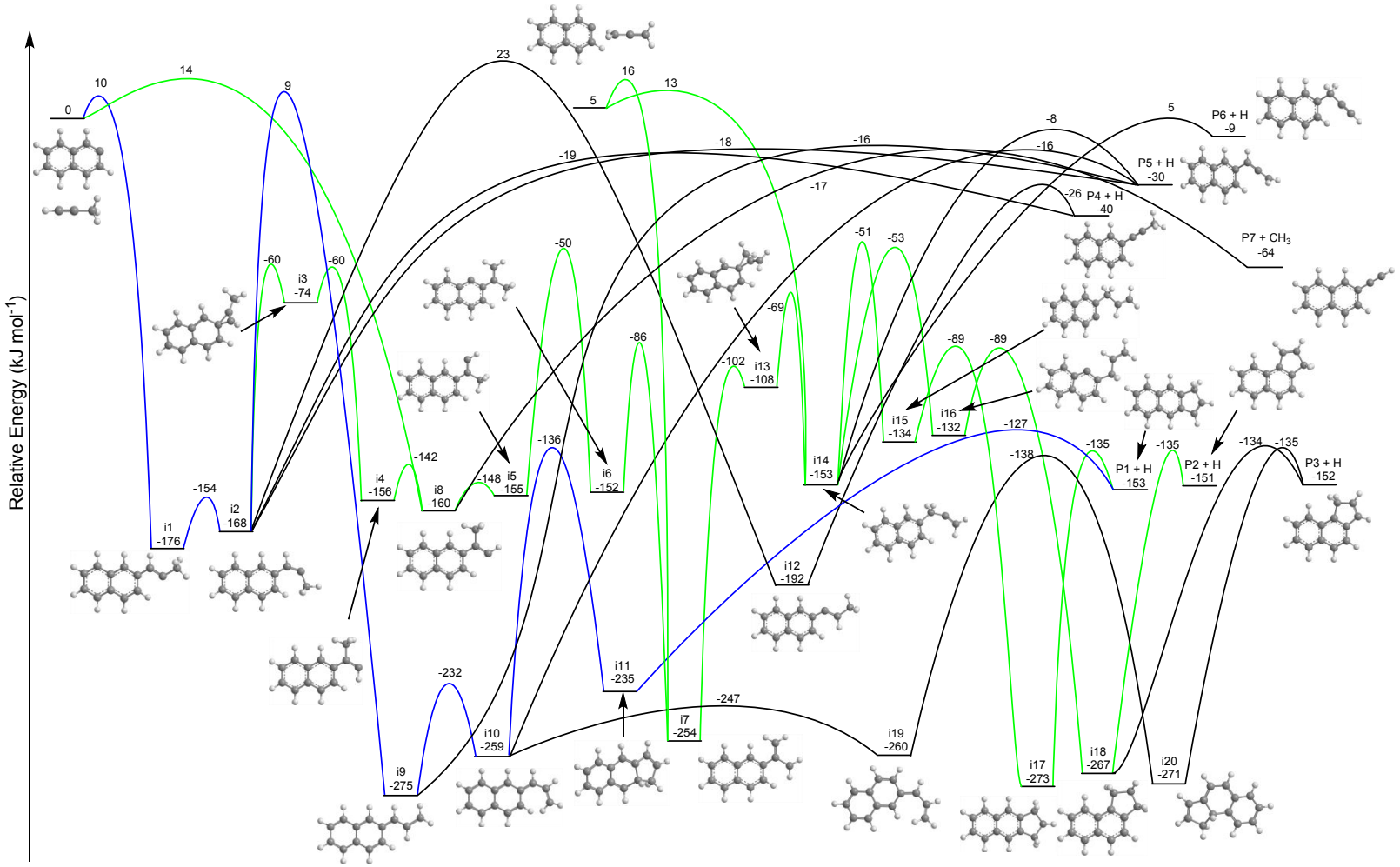

Figure 6. Potential energy surface (PES) for the 2-naphthyl ($C_{10}H_7^{\bullet}$) reaction with allene/methylacetylene (C_3H_4). This PES was calculated at the G3(MP2,CC)//B3LYP/6-311G(d,p) level of theory for the channels leading to 1*H*-benz[*f*]indene (**p1**), 3*H*-benz[*e*]indene (**p2**), 1*H*-benz[*e*]indene (**p3**), 2-(prop-1-yn-1-yl)naphthalene (**p4**), 2-(propa-1,2-dien-1-yl)naphthalene (**p5**), 2-(prop-2-yn-1-yl)naphthalene (**p6**) and 2-ethynyl-naphthalene (**p7**). The relative energies are given in kJ mol^{-1}. Blue and green lines indicate two alternative pathways leading to the formation of benzindene molecules (**p1** and **p2**) observed in the present work.

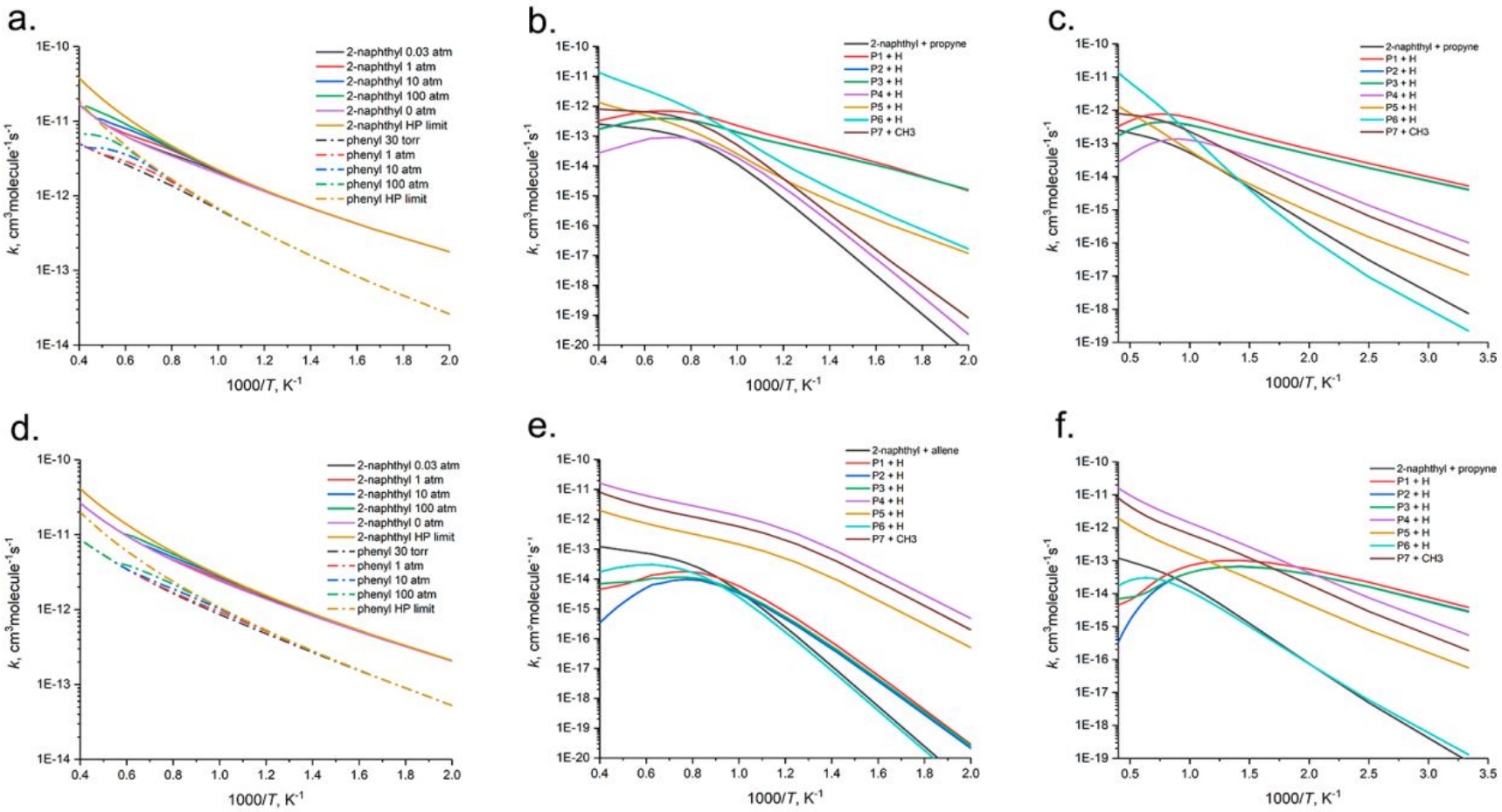

Figure 7. Calculated total and individual rate constants for the 2-naphthyl + C_3H_4 reactions: a. total rate constants for 2-naphthyl + allene at different pressures, total rate constants for the phenyl + allene reaction (Ref. 77) are shown for comparison; b. and c. rate constants for various bimolecular product channels of the 2-naphthyl + allene reaction at 0.03 atm and at zero pressure limit, respectively; d. total rate constants for 2-naphthyl + methylacetylene at different pressures, total rate constants for the phenyl + methylacetylene reaction (Ref. 77) are shown for comparison; e. and f. rate constants for various bimolecular product channels of the 2-naphthyl + methylacetylene reaction at 0.03 atm and at zero pressure limit, respectively. Note that the blue (**p2**) and green (**p3**) curves merge at panels b. and c.

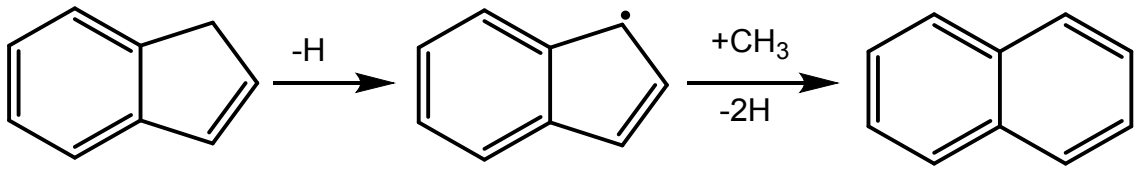

Scheme 5. Conversion of indene to naphthalene via H-loss and the reaction with methyl radical (CH_3).

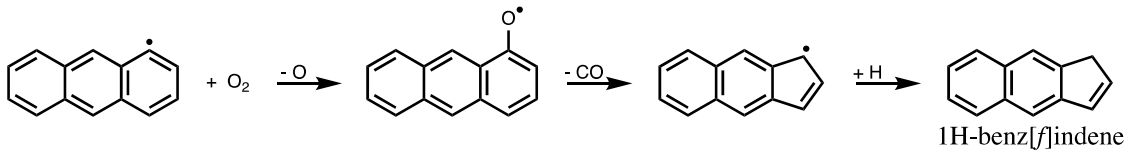

Scheme 6. Formation of 1*H*-benz[*f*]indene from 1-anthryl radical via the reaction with O_2, CO loss and hydrogen addition processes.

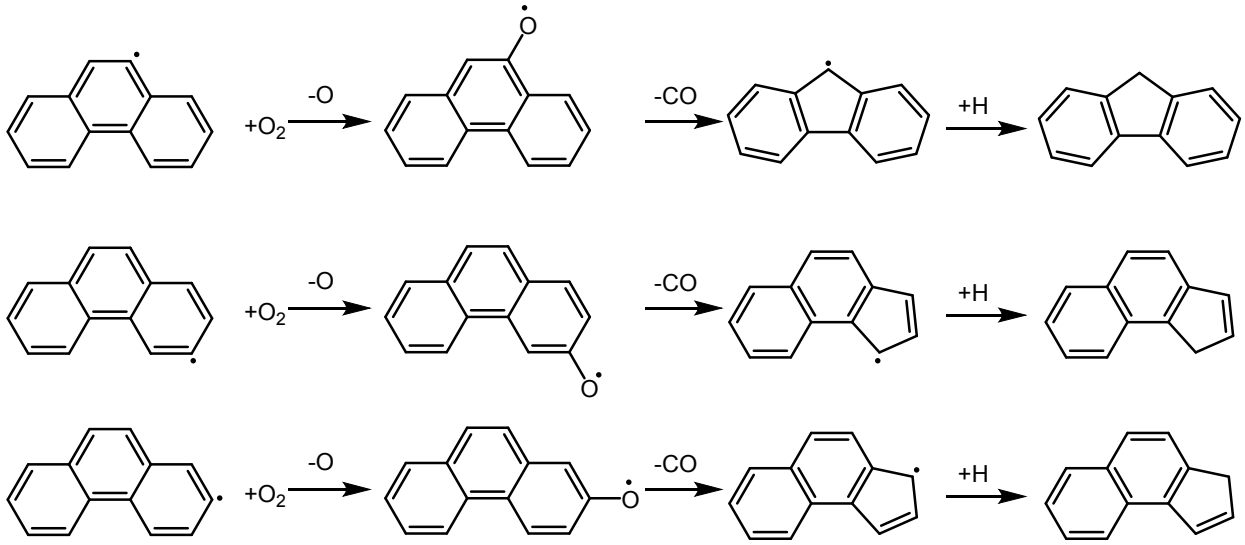

Scheme 7. Formation of PAHs carrying a five-member ring from phenanthrenyl radicals via the reaction with O_2, CO loss and hydrogen addition processes.

Table of contents entry

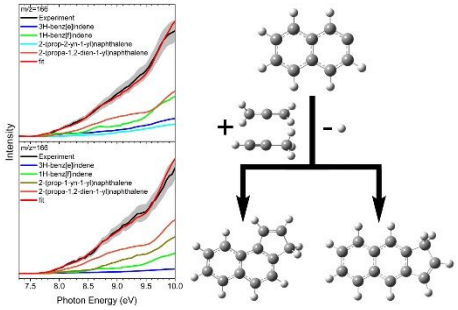

The reaction of aryl radicals with allene/methylacetylene leads to five-membered ring addition in PAH growth processes.

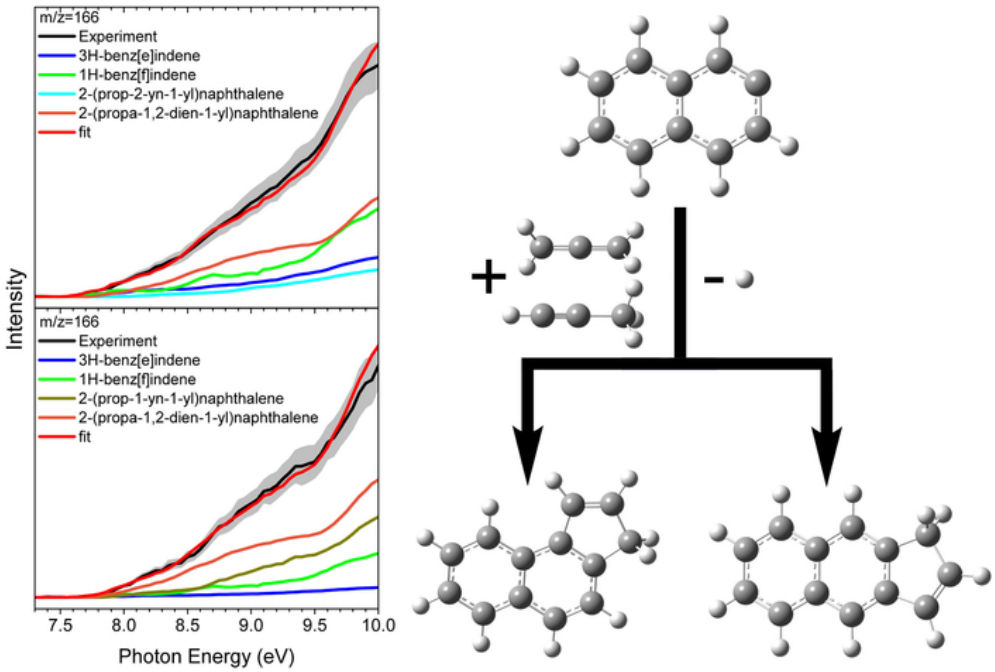

59x39mm (300 x 300 DPI)